Electro-oxidation of formic acid catalyzed by FePt nanoparticles†

Wei Chen,[a] Jaemin Kim,[b] Shouheng Sun[b] and Shaowei Chen*[a]

The electrocatalytic oxidation of formic acid at a gold electrode functionalized with FePt nanoparticles was studied by cyclic voltammetry (CV) and electrochemical impedance spectroscopy (EIS) in a mixed solution of 0.1 M HCOOH and 0.1 M HClO$_4$. The FePt bimetallic nanoparticles, with a mean diameter of 3 nm, were prepared by a chemical reduction method. The Au/FePt nanostructured electrode was prepared firstly by the deposition of FePt nanoparticles onto a clean Au electrode surface, followed by ultraviolet ozone treatment to remove the organic coating. In CV measurements, two well-defined anodic peaks were observed at +0.20 and +0.51 V (*vs.* a Ag/AgCl quasi-reference). The anodic peak at +0.20 V was attributed to the oxidation of HCOOH to CO$_2$ on surface unblocked by CO, whereas the peak at +0.51 V was ascribed to the oxidation of surface-adsorbed CO (an intermediate product of HCOOH oxidation) and further oxidation of bulk HCOOH. From the onset potential and current density of the electro-oxidation of HCOOH, FePt nanoparticles exhibit excellent electrocatalytic activities as compared to Pt and other metal alloys. EIS measurements were carried out to further examine the reaction kinetics involved in the HCOOH electro-oxidation. The EIS responses were found to be strongly dependent on electrode potentials. At potentials more positive than −0.25 V (*vs.* Ag/AgCl), pseudo-inductive behavior was typically observed. At potentials between +0.3 and +0.5 V, the impedance response was found to reverse from the first quadrant to the second quadrant; such negative Faradaic impedance was indicative of the presence of an inductive component due to the oxidation of surface-adsorbed CO. The impedance responses returned to normal behavior at more positive potentials (+0.6 to +0.9 V). The mechanistic variation was attributed to the formation of different intermediates (CO or oxygen containing species) on the electrode surface in different potential regions. Two equivalent circuits were proposed to model these impedance behaviors.

Introduction

There has been an increasing interest in the development of efficient fuel cells due to the need for alternative energy sources with high energy density, low operating temperature and low environmental pollution. For fuel cells, aqueous solutions of formic acid and methanol represent two potential, attractive energy sources because of the ease of handling, transportation and storage in comparison to those of gaseous or liquid hydrogen.[1] Previous studies have showed that formic acid can be oxidized at less positive potentials than methanol and that crossover of formic acid through the polymer membrane is lower than that of methanol.[2–4] Thus, a great deal of research effort has been focused on the electrochemical properties of formic acid, which serves as an important model system for studying electrochemical oxidation of small organic molecules.[5–13]

Fuels based on the oxidation of small organic molecules require electrocatalysts to achieve the current density needed for commercial fuel cell applications. For instance, single crystal and polycrystalline platinum, palladium, rhodium and gold electrodes have been used extensively as catalysts for the electro-oxidation of formic acid.[14–16] Among these metal catalysts, platinum shows the highest catalytic activity for electro-oxidation of methanol and formic acid. In order to enhance the oxidation efficiency and reduce costs, Pt-based alloy catalysts with various transition metals such as Pt–Ru,[17–20] Pt–Ni,[21,22] Pt–Sn,[23,24] Pt–Co,[25–26] Pt–Pb,[27] Pt–Bi,[28,29] Pt–Pd,[30,31] Pt–Ti[32] and Pt–Cr[33] have been prepared and studied as possible catalysts for the electro-oxidation of small organic molecules. It is widely accepted that formic acid is oxidized to CO$_2$ *via* the so-called dual-pathway mechanism, which involves a reactive intermediate (direct path) or adsorbed CO as a poisoning intermediate species (indirect path). In this complicated reaction, carboxylic acid species (HCOO) is generally proposed as the reactive intermediate and adsorbed CO is assigned as the poisoning species. These results have been identified by *in situ* Surface-Enhanced IR Absorption Spectroscopy (SEIRAS).[34–38]

It is well-known that when pure platinum is used as the catalyst, it will be rapidly poisoned by the adsorption of CO produced during the oxidation of HCOOH. However, many

[a] Department of Chemistry and Biochemistry, University of California, Santa Cruz, CA, 95064, USA. E-mail: schen@chemistry.ucsc.edu; Fax: +1-831-459-2935; Tel: +1-831-459-5841
[b] Department of Chemistry, Brown University, Providence, RI, 02912, USA
† Electronic supplementary information (ESI) available: TEM image and XRD spectrum of the FePt nanoparticles. See DOI: 10.1039/b603045a

This journal is © the Owner Societies 2006

Phys. Chem. Chem. Phys., 2006, **8**, 2779–2786 | 2779

investigations have shown that some Pt-based alloy catalysts exhibit enhanced tolerance of CO and, consequently, improved electrocatalytic activities compared to those with platinum alone. For instance, two mechanisms have been proposed to account for the promotional effect of Pt–Ru alloy catalysts. One is the so-called bifunctional mechanism,[39–41] in which the role of ruthenium is to dissociate water to form adsorbed OH species, which then reacts with adsorbed CO to generate CO_2. Another explanation is the electronic ligand-effect mechanism, *i.e.* the electronic properties of platinum are modified by Pt–Ru orbital overlaps so that the binding strength of CO adsorbed on Pt is weakened, leading to the enhancement of electrocatalytic activities for formic acid electro-oxidation.[17,42]

Due to the high proportion of surface to bulk atoms, the surface area and the reactivity of nanostructured metal materials are significantly higher than those of the corresponding bulk metals, rendering them ideal candidates in catalytic applications. In fact, currently, many studies of the electrocatalytic oxidation of methanol and formic acid are focused on Pt and Pt-base alloy nanoparticles.[13,32,33,35] For instance, Watanabe *et al.*[43–45] prepared Fe–Pt alloy thin films using the magnetron sputtering deposition method and found that such alloy films exhibited high CO-tolerance toward H_2 oxidation or O_2 reduction. Such materials will be candidates for CO-tolerant alloyed catalysts in fuel cells. However, to the best of our knowledge, there have been no studies on methanol or formic acid oxidation catalyzed by FePt alloy nanoparticles.

Here, we use monodispersed FePt nanoparticles as catalysts for the electro-oxidation of formic acid. These FePt nanoparticles were prepared by a simultaneous decomposition of iron pentacarbonyl, $Fe(CO)_5$, and reduction of platinum acetylacetonate, $Pt(acac)_2$, in the presence of oleic acid and oleylamine.[46] FePt nanoparticles with an average diameter of ~ 3 nm were deposited onto a gold electrode surface (denoted as Au/FePt electrode) and were found to be efficient in the electro-catalytic oxidation of formic acid, with a high tolerance of CO poisoning. The onset potential and current density for the HCOOH oxidation, as evidenced by voltammetric and electrochemical impedance spectroscopic studies, demonstrate that the FePt nanoparticles may be used as a powerful catalyst for the electro-oxidation of formic acid fuel.

Experimental

Materials

Perchloric acid ($HClO_4$, Fisher, 99.999%) and methanol (CH_3OH, ACROS, 99.999%) were used as received. Water was supplied by a Barnstead Nanopure water system (18.3 $M\Omega$). All solutions were deaerated by bubbling ultra-high-purity N_2 for 20 min and protected with a nitrogen atmosphere during the entire experimental procedure.

The FePt nanoparticles were prepared according to a previous publication, where the composition of the particles was controlled at $Fe_{20}Pt_{80}$ to ensure particle stability in strong acid media.[46] Briefly, under a gentle flow of N_2, Pt(acetylacetonate)$_2$ (0.5 mmol), 1,2-hexadecanediol (1.5 mmol) and dioctyl ether or benzyl ether (20 mL) were mixed at room temperature and heated to 100 °C. Oleic acid (0.5 mmol), oleylamine (0.5 mmol) and $Fe(CO)_5$ (1.0 mmol) were added and the mixture was heated to reflux (297 °C) for 30 min. (Note: N_2 was kept flowing through the reaction system to ensure the Pt-rich $Fe_{20}Pt_{80}$ nanoparticles were formed. This was different from the previous synthesis in which the reaction was run under a blanket of N_2.) The heat source was removed and the reaction mixture was cooled down to room temperature, at which point the reaction system was opened to the ambient environment. The black product was precipitated by adding ethanol (40 mL) and separated by centrifugation. The supernatant was discarded and the black precipitate was dispersed in hexane (25 mL) in the presence of oleic acid (0.05 mL) and oleylamine (0.05 mL). Then, ethanol (20 mL) was added to the dispersion and the suspension was centrifuged again. The precipitation was re-dispersed by hexane. The average particle core diameter was estimated to be 3 nm based on transmission electron microscopy measurements (see ESI†). From the X-ray diffraction (XRD) pattern of the FePt nanoparticles, which is also included in the ESI†, the alloy structure of the resulting FePt particles can be clearly identified.

Preparation of the Au/FePt electrode

A polycrystalline gold disk electrode (sealed in glass tubing) was firstly polished with alumina slurries (0.05 μm) and then cleansed by sonication in 0.1 M HNO_3, H_2SO_4 and Nanopure water for 10 min, successively. FePt nanoparticles (10 μL) dissolved in hexane (0.9 mg mL^{-1}) was then deposited onto the Au electrode surface by a Hamilton microlitre syringe. The particle film was dried by a gentle nitrogen flow for *ca.* 2 min. The surface coverage of this particle assembly was estimated to be *ca.* 9 layers by assuming a fully intercalated nanoparticle assembly. The organic protecting ligands were then removed by oxidation in an ultraviolet ozone (UVO) chamber (Jelight Company, Inc., Model 42) for 15 min. The particle film was then rinsed with excessive Nanopure water and ethanol to remove remaining organic deposits.

Electrochemistry

Voltammetric measurements were carried out with a CHI 440 electrochemical workstation. The Au/FePt electrode was used as the working electrode. An Ag/AgCl wire and a Pt coil were used as the reference and counter electrodes, respectively. All electrode potentials in the present study will be referred to this Ag/AgCl quasi-reference. Electrochemical impedance spectroscopy (EIS) measurements were carried out using an EG&G PARC Potentiostat/Galvanostat (model 283) and a Frequency Response Detector (model 1025). The impedance spectra were recorded between 100 kHz and 10 mHz, with the amplitude (rms value) of the ac signal being 10 mV.

Results and discussion

1. Electrochemical characterizations of the electrodes

Fig. 1 shows the cyclic voltammograms of the naked Au electrode and the FePt particles-modified Au electrode before and after UVO treatment in 0.1 M $HClO_4$, at a potential sweep

2780 | *Phys. Chem. Chem. Phys.*, 2006, **8**, 2779–2786

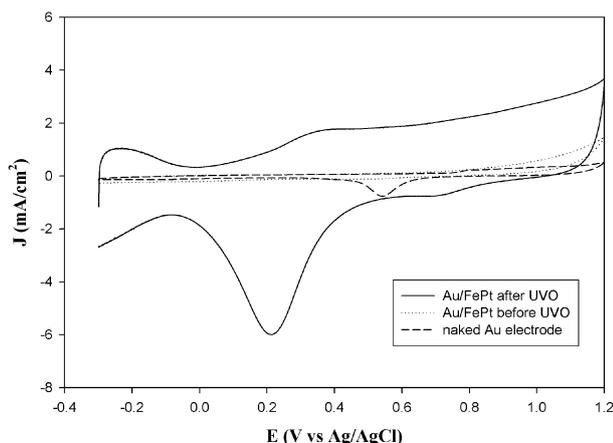This journal is © the Owner Societies 2006

Fig. 1 Cyclic voltammograms of the naked Au electrode (--), FePt particles modified Au electrode before (···) and after (—) UVO treatment in 0.1 M HClO$_4$. Potential scan rate = 0.1 V s^{-1}. Electrode surface area = 0.119 mm^2.
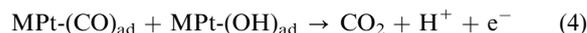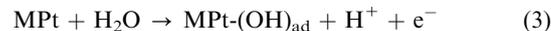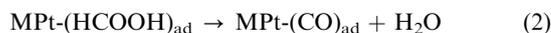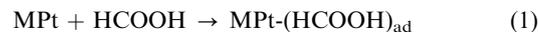
rate of 0.1 V s^{-1}. For the naked Au electrode, the Au oxidation current at potentials above +0.8 V can be clearly seen. In the cathodic potential sweep, there is a voltammetric peak at +0.54 V corresponding to the reduction of the Au oxide. Such voltammetric responses have been observed previously at polycrystalline Au electrode surfaces.[47] However, upon the deposition of FePt particles onto the Au electrode surface, the voltammetric features observed above become substantially suppressed. This may be ascribed to the hydrophobic nature of the organic protecting-layers on the particles that render the Au electrode surface inaccessible by electrolyte ions. In addition, the essentially featureless response also suggests that the FePt particles remain electrochemically inactive within this potential window. However, after the organic protecting ligands were removed by the UVO treatment, the voltammetric response exhibited a drastic variation (Fig. 1). Firstly, at low potentials, there is a pair of broad current peaks between +0.08 V and −0.3 V which can be attributed to the adsorption–desorption of hydrogen on the metallic Pt surface. Secondly, a reduction current peak can be seen at +0.21 V in the cathodic potential sweep that may be assigned to the reduction of platinum oxides formed at more positive potentials during the anodic potential scan. The observed CV feature is very similar to that for polycrystalline Pt electrodes.[43,45,47] Igarashi et al. attributed the CV resemblance of Pt-based alloys with polycrystalline Pt to the formation of a Pt skin layer after the electrochemical process.[43–45] Such an effect may also explain the voltammetric behaviors observed above for the FePt nanoparticles. The electrocatalytic activity of this functionalized electrode was then examined for formic acid oxidation.

2. Electrocatalytic activity for formic acid oxidation

It is well-known that the second metal in Pt-based alloy catalysts can promote the electro-oxidation of small organic molecules. On the basis of previous results of the reaction kinetics in methanol or formic acid electro-oxidation at binary metal electrodes,[48–50] a similar effect might be suggested for

FePt nanoparticles from the CV investigation in Fig. 1. The reaction mechanism for formic acid oxidation on Pt-based alloy (MPt) nanoparticle surfaces is proposed as below:

For the indirect oxidation path

$$MPt + HCOOH \rightarrow MPt\text{-}(HCOOH)_{ad} \qquad (1)$$

$$MPt\text{-}(HCOOH)_{ad} \rightarrow MPt\text{-}(CO)_{ad} + H_2O \qquad (2)$$

$$MPt + H_2O \rightarrow MPt\text{-}(OH)_{ad} + H^+ + e^- \qquad (3)$$

$$MPt\text{-}(CO)_{ad} + MPt\text{-}(OH)_{ad} \rightarrow CO_2 + H^+ + e^- \qquad (4)$$

For the direct oxidation path

$$MPt\text{-}(OH)_{ad} + HCOOH \rightarrow CO_2 + H_2O + H^+ + e^- \qquad (5)$$

The first step entails the adsorption of HCOOH onto the surface of the nanocatalysts. These HCOOH molecules then undergo rapid dissociation into water and CO, and the latter binds strongly to the catalyst surface (i.e., the poisoning effect, step 2). The CO molecules can be further oxidized into CO$_2$ (step 4) by reacting with the hydroxyl species generated by water electrolysis on the catalyst surface (step 3). It is suspected that the electro-oxidation of HCOOH on the FePt particle surface also follows this mechanism (vide infra). By contrast, in the direct oxidation path (step 5), electro-oxidation of HCOOH will be initiated by surface-adsorbed hydroxyl species (step 3) into CO$_2$ and H$_2$O.

Fig. 2 presents the steady-state cyclic voltammograms of the Au/FePt electrode in 0.1 M HCOOH and 0.1 M HClO$_4$. It can be seen that the anodic current is substantially greater than that in 0.1 M HClO$_4$ alone (dotted line, which is identical to the solid curve in Fig. 1), suggesting that the voltammetric features are arising from the electro-oxidation of HCOOH. This observation is in good agreement with those using Pt and other Pt-based alloy electrodes.[38–51] There are three anodic peaks at about +0.2, +0.51 and +1.06 V in the anodic scan. In the cathodic scan, a very large peak at +0.18 V is observed. It is known that formic acid is either electro-oxidized directly to CO$_2$ by dehydrogenation (step 5), or dissociates spontaneously to produce CO which then becomes oxidized to CO$_2$ (steps 1–4). The poisoning CO species are usually formed within the
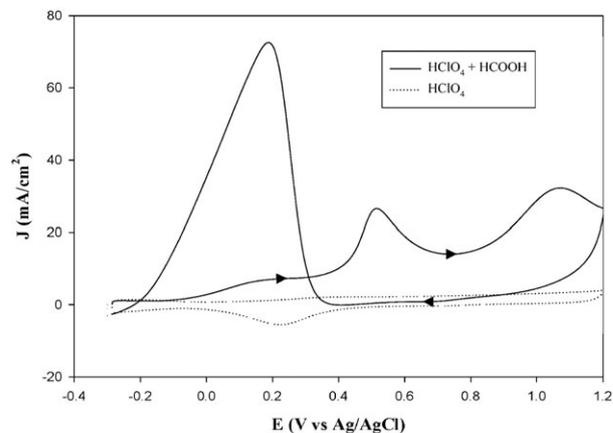

Fig. 2 Steady-state cyclic voltammograms of the Au/FePt electrode in 0.1 M HCOOH + 0.1 M HClO$_4$ (—) and in 0.1 M HClO$_4$ (···). Potential scan rate 0.1 V s^{-1}.

hydrogen region as well as in the double-layer region. It can be seen from Fig. 2 that the hydrogen adsorption–desorption currents are significantly inhibited at the Au/FePt electrode in the presence of HCOOH, indicating the surface active sites have been blocked noticeably by adsorbed CO species. Since the CO formation from formic acid does not generate Faradaic current (step 2), the anodic peaks in Fig. 2 are most probably arising from the oxidation of formic acid or CO. Of these, the anodic current peak at +0.2 V can be attributed to the oxidation of HCOOH to CO_2 on surface active sites that have not been poisoned by CO (direct path in step 5). The anodic current peak at +0.51 V may arise from the oxidation of the adsorbed CO and formic acid as a consequence of the release of surface active sites by CO removal (step 4). With further increase in electrode potentials, platinum oxides begin to form and the electrode becomes inactive. At higher potentials, some catalytically active surface oxides can be formed, leading to the anodic current peaks at +1.06 V. In the subsequent cathodic scan, only one voltammetric peak can be seen at +0.18 V, with a significantly greater peak current that can be attributed to the direct oxidation of formic acid, through an active intermediate, into CO_2 (the direct path, *vide ante*). In this, it should be noted that, in the cathodic scan, formic acid begins to be oxidized only when the potential moves to about +0.36 V. This phenomenon can be attributed to the effect of metal surface oxides of different valence states on formic acid oxidation. For instance, previous studies[52–54] have demonstrated that at high oxidation states, some Pt surface oxides (*i.e.*, $Pt(OH)_3$ and PtO_2) formed at high potentials may actually be poisoning species. Thus, formic acid can be oxidized only when these surface oxides are reduced at low potentials, so that the electrode surface active sites are restored. The enhanced peak current of formic acid oxidation observed in the reverse cathodic scan, as compared to that in the anodic scan, can then be ascribed to the fact that at these potentials, the surface-adsorbed CO species would have been oxidized to CO_2. Consequently, the HCOOH catalytic reaction actually follows the direct path.

Usually, onset potential and current density are the two important parameters to compare the activities of electrocatalysts for the electro-oxidation of formic acid or methanol. For instance, Pt and PtRu nanoparticle electrodes exhibited onset potentials of +0.10 and +0.16 (*vs.* Ag/AgCl in saturated NaCl) for the electro-oxidation of formic acid, respectively.[28] It can be seen from Fig. 2 that for formic acid oxidation on the FePt nanoparticle electrode, the onset potential is −0.17 V (*vs.* Ag/AgCl quasi-reference), which is about +0.13 V (*vs.* Ag/AgCl in saturated NaCl) by using the Au oxidation peak as the calibration point. In comparison to the performance of Pt and PtRu nanoparticles,[28] the FePt nanoparticle-functionalized electrode exhibits comparable onset potential for formic acid oxidation. These results also agree well with the excellent CO tolerance of the FePt alloy.[43–45] However, from the current intensity of formic acid oxidation in the positive and negative scans, it can be seen that the electrode is heavily poisoned by adsorbed CO under the present experimental conditions. Actually, we found that the electrocatalytic activity of the electrode was sensitive to the thickness of the FePt particle film. For instance, for FePt monolayers (by Langmuir–Blod-

gett deposition), the electrocatalytic activities toward formic acid oxidation were dramatically enhanced. Under the present conditions, the CO adsorbed on the inner FePt particle layers may be difficult to remove by electro-oxidation. Such properties are currently under investigation and the results will be reported in due course.

3. Electrochemical impedance studies

Further studies of the electro-oxidation of HCOOH at the Au/FePt electrode were carried out with electrochemical impedance measurements. Fig. 3 shows the Nyquist complex-plane impedance spectra of the Au/FePt electrode in 0.1 M HCOOH and 0.1 M $HClO_4$ at various electrode potentials. In the top panel, at $E = -0.3$ V, the impedance spectrum shows a large arc, with the diameter significantly greater than those at more positive potentials, which can be attributed to the slow reaction rate of formic acid oxidation. It is most probable that the presence of resistive and capacitive components in the equivalent circuit arises from the double-layer effects. From the CV measurements in Fig. 2, it can be seen that at −0.3 V, formic acid dissociates spontaneously to form CO (step 2), which adsorbed readily on the Au/FePt electrode surface. Thus, the slow reaction kinetics of formic acid oxidation as inferred from the impedance measurements can be ascribed to poisoning by intermediate CO, which blocks continuing adsorption and dehydrogenation of HCOOH on the electrode surface. With a further increase of the electrode potential up to +0.1 V, the impedance spectra exhibit a drastic variation: (i) in addition to the arc in the first quadrant (at high frequency), a smaller one starts to emerge in the fourth quadrant (at low frequency); and (ii) the diameter of both arcs decreases sharply with increasing electrode potential. Such pseudo-inductive behavior has also been observed in methanol electro-oxidation.[55,56] Initially, the reaction sites on the electrode surface are occupied by adsorbed CO generated from formic acid dehydrogenation (step 2). At higher potentials, the weakly-bound CO will be oxidized, leading to the recovery of the surface reaction sites where electro-oxidation of formic acid can then take place. It should be recognized that the low-frequency intersect of the impedance spectra with the x axis (*i.e.*, charge-transfer resistance) also decreases with increasing electrode potentials, signifying enhanced reaction kinetics of the overall electro-oxidation of formic acid.[57–58] These observations are also in agreement with the voltammetric results in Fig. 2, where the broad anodic peak at *ca.* +0.2 V is ascribed to the direct oxidation of formic acid to CO_2 (*vide ante*).

Fig. 3 (middle panel) depicts the impedance plots at potentials between +0.3 V and +0.5 V. An interesting feature of the impedance plot can be observed in this potential range; when the potential is more positive than +0.3 V, negative Faradaic impedance can be observed that are drastically different from the normal Nyquist plots under other potentials (*e.g.*, top and bottom panels). Namely, the impedance spectra now show up in the second quadrant instead of the conventional first one. Again, similar behaviors have also been observed during electro-oxidation of methanol and formic acid on Pt and other Pt-based alloy electrodes.[29,55,56] Such a rapid transition from positive to negative Faradaic impedance suggests the presence
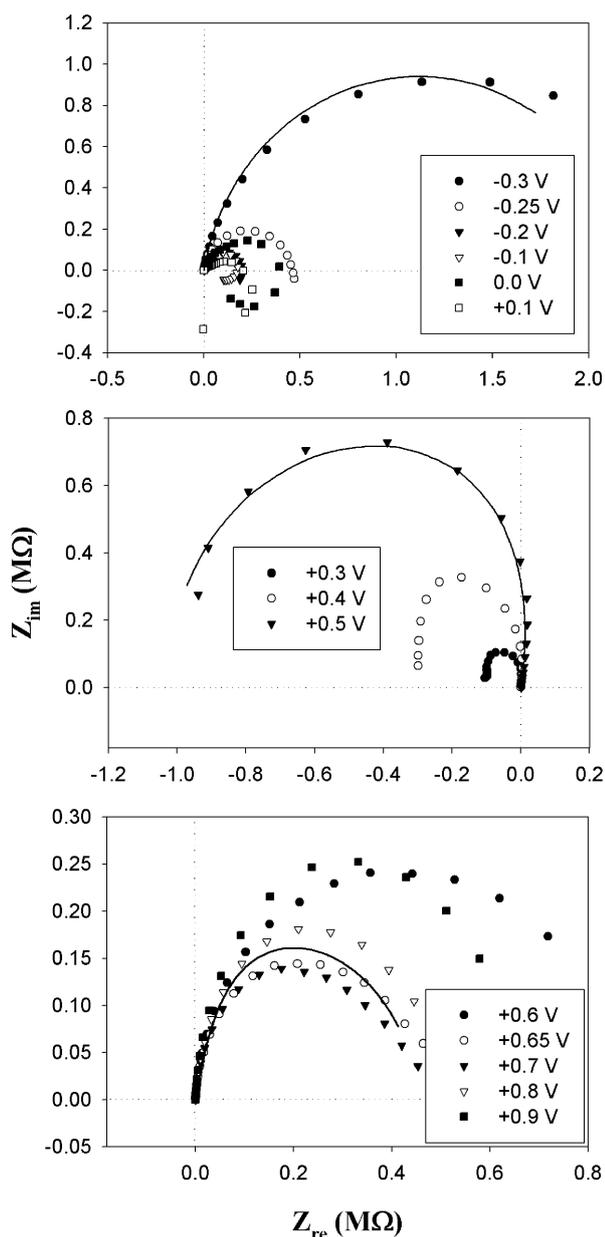
Fig. 3 Complex-plane electrochemical impedance plots (Nyquist plots) of the Au/FePt electrode in 0.1 M HCOOH + 0.1 M HClO$_4$ at various electrode potentials, which are given in the figure legends. The solid lines show some representative fits to the experimental data by the equivalent circuit in Fig. 5: −0.3 V (top); +0.5 V (middle); and +0.65 V (bottom).

of an inductive component.[59] Inductive behavior is often observed in systems involving adsorbed intermediates or metal surface corrosion.[55,56,59,60] Here, the negative Faradaic impedance can be explained by the formation of chemisorbed hydroxyl species within this potential range (step 3), which competes for surface adsorption sites against the poisoning intermediates (CO) and, at the same time, enhances their oxidative removal from the electrode surface (step 4). It is worth noting from the CV measurements in Fig. 2 that between the potentials of +0.3 and +0.5 V, adsorbed CO

begins to be oxidized, leading to high activities of the electrode surface for CO oxidation in this potential range. Usually, the hydroxyl species is considered as the oxygen-donating species for adsorbed CO. Thus, the impedance results agree well with those of CV measurements; and both experimental results indicate that the formation of chemisorbed hydroxyl significantly enhances the oxidation of surface-adsorbed CO.

In addition, from Fig. 3 (bottom panel), it can be seen that at potentials more positive than +0.6 V, the impedance plots return to normal behaviors and the diameter of the arc firstly decreases (from +0.6 to +0.7 V) and then increases (+0.7 to +0.9 V) with increasing potentials. The increase of the arc diameter above +0.7 V is probably due to the formation of Pt surface oxides, which leads to the increase of the charge-transfer resistance for formic acid oxidation.

Fig. 4 shows the corresponding Bode plots of the Au/FePt electrode in 0.1 M HCOOH + 0.1 M HClO$_4$ within different potential ranges (indicated in the figure legends). The kinetic process of the electrode reaction can also be evaluated from the variation of the effective phase angle with electrode potentials. It can be seen from the top panel that there exists a maximum phase angle (somewhat less than −90°, as anticipated from a purely capacitive element) at a characteristic frequency (f_1) for all Bode plots. This frequency, and hence the corresponding electrochemical reaction rate, increases with electrode potentials,[55,58] as it represents the time constant for the overall electrochemical reaction. When the potential is more positive than −0.25 V, negative phase angles start to appear at low frequencies, signifying that the reaction kinetics changes from resistive behaviors to pseudo-inductive behaviors.[55,58] Additionally, the frequency (f_2) at zero phase angle also increases with increasing electrode potential; again, indicative of enhanced reaction kinetics as mentioned above.

In the potential range from +0.3 V to +0.5 V (middle panel), however, an abrupt jump between the positive and negative values of the phase angle was observed. This interesting phenomenon corresponds to the transition to negative faradaic impedance as shown in the Nyquist plots in Fig. 3 (middle panel). It can be ascribed to the difference of potential dependency between the dehydrogenation reaction of formic acid (step 2) and the electro-oxidation of adsorbed CO (step 4). The reaction rates of these two processes are typically reflected by a maximum in the high and low frequency region, respectively. As mentioned above, generally, the latter (step 4) is a slower process (and therefore the rate-determining step) and more sensitive to electrode potentials than the former (though both frequencies increase with increasing electrode potentials). At sufficiently high electrode potentials, the reaction rate of step 4 starts to be comparable to that of step 2, leading to the abrupt change of the phase angle. Such behavior is very similar to that observed in methanol electro-oxidation.[55] When the potential is more positive than +0.6 V, surface-adsorbed CO is removed almost completely and there is only one positive maximum of phase angle in the Bode plots (bottom panel).

From the above CV and impedance results (Fig. 3 and 4), the electrode reaction for formic acid oxidation can be derived in different potential regions. The equivalent circuit, shown in Fig. 5(A), can be used to fit the above impedance data at
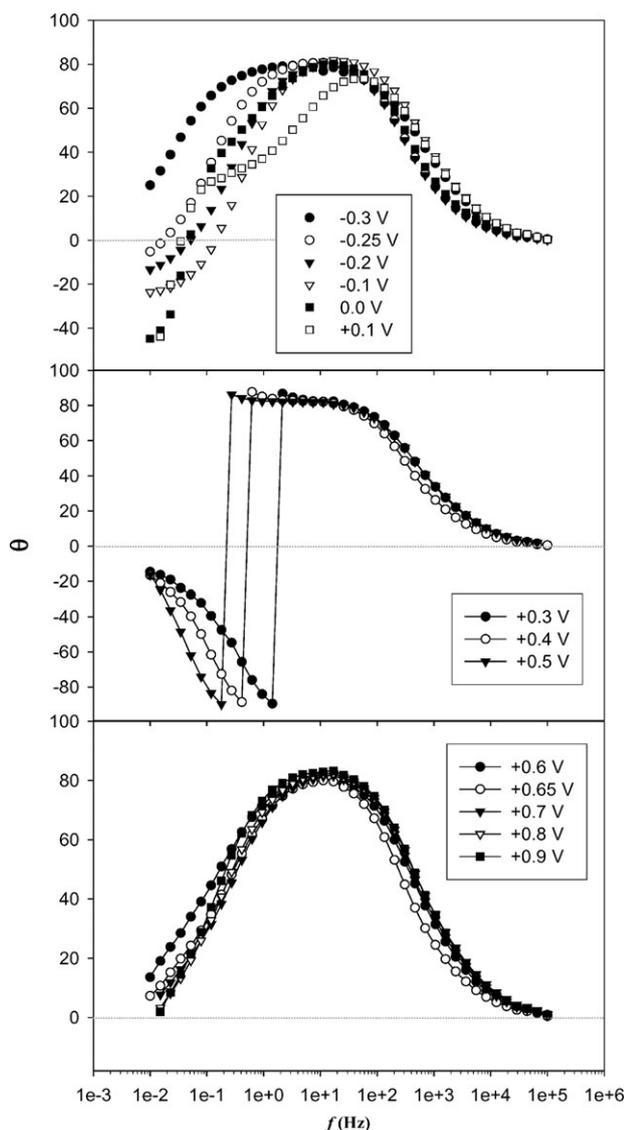
This journal is © the Owner Societies 2006

Phys. Chem. Chem. Phys., 2006, **8**, 2779–2786 | 2783

Fig. 4 Bode plots of the electrochemical impedance of the Au/FePt electrode in 0.1 M HCOOH + 0.1 M HClO$_4$ at various electrode potentials, which are given in the figure legends.

Fig. 5 Equivalent circuits for the electro-oxidation of formic acid at the Au/FePt electrode in varied potential regimes: (A) at potentials more negative than +0.3 V or more positive than +0.5 V; and (B) at potentials between +0.3 V and +0.5 V.

chemisorbed hydroxyl species. Thus, a component corresponding to this reaction should be included in the equivalent circuit. The impedance data in this potential range were then fitted using the equivalent circuits shown in Fig. 5(B),[63] where C_o and R_o represent the reaction capacitance and resistance arising from the oxidation of adsorbed CO on the Au/FePt electrode surface. A representative fit using such a circuit is depicted in the middle panel of Fig. 3 (+0.5 V).

Table 1 summarizes the fitting results of R_S, R_{CT}, CPE, n, C_o and R_o at different potentials by using the equivalent circuits in Fig. 5, where n is a parameter for CPE, and at $n = 1$, the CPE can be considered as a capacitor. From Table 1, it can be seen that the values of R_S (solution resistance), CPE, and n are virtually invariant within the entire potential range under study (-0.3 V to $+0.9$ V). The fact that $n \approx 0.9$ at all electrode potentials indicates that the CPE in this study is close to pure capacitance. However, it is interesting to note that the charge transfer resistance (R_{CT}) exhibits a clear dependence on electrode potentials, which is depicted in Fig. 6. At $E = -0.3$ V, R_{CT} is more than 2 MΩ; whereas at a slightly more positive potential, $E = -0.25$ V, R_{CT} decreases sharply by a factor of

potentials more negative than +0.3 V or more positive than +0.5 V. Two representative fits are shown in the top (-0.3 V) and bottom ($+0.65$ V) panels of Fig. 3. It can be seen that both fits are excellent. Here, R_S is the solution resistance, CPE (constant-phase element) and R_{CT} are the capacitance (which represents the double layer capacitance) and charge transfer resistance, respectively. It has often been observed that the impedance spectrum of a solid electrode may be distorted as a consequence of the roughness of the catalytic layer or a current constriction effect.[55,57,58,61,62] In the present study, the depressed semicircles in the complex-plane impedance plots can be ascribed to the high surface roughness of the electrode modified with FePt nanoparticles. On such a porous solid electrode, the double layer impedance often exhibits CPE characteristics instead of behaving like a pure capacitor.

In the potential range between +0.3 V and +0.5 V, the adsorbed CO begins to oxidize thanks to the formation of
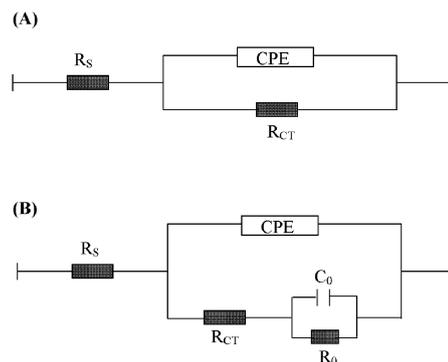
Table 1 Fitting parameters of the electrochemical impedance for Au/FePt electrode at various potentials[a]

E/V	R_S/Ω	R_{CT}/kΩ	CPE/μF	n	C_o/μF	R_o/kΩ
-0.3	180.1	2233.0	2.58	0.89	—	—
-0.25	260.7	450.3	2.44	0.93	—	—
-0.2	263.2	193.9	2.30	0.94	—	—
-0.1	184.0	138.1	1.39	0.96	—	—
0	255.4	233.0	2.23	0.92	—	—
$+0.1$	164.9	100.5	4.54	0.79	—	—
$+0.3$	174.8	-118.5	2.72	0.88	5.20	0.14
$+0.4$	263.7	-373.3	2.37	0.91	3.73	0.45
$+0.5$	177.8	-1122.0	2.28	0.91	0.97	1.39
$+0.6$	172.6	626.4	3.07	0.89	—	—
$+0.65$	271.6	398.5	2.83	0.89	—	—
$+0.7$	176.8	379.6	2.52	0.90	—	—
$+0.8$	176.0	215.9	2.01	0.93	—	—
$+0.9$	177.9	641.1	1.97	0.93	—	—

[a] Experimental data were measured in 0.1 M HCOOH + 0.1 M HClO$_4$ (Fig. 3) and fitted by using the equivalent circuits shown in Fig. 5.
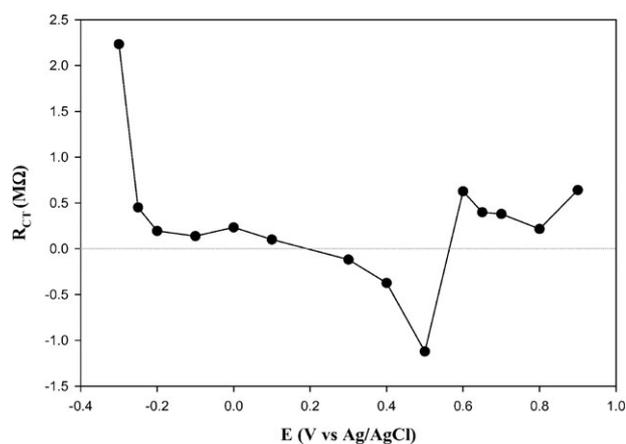
Fig. 6 Dependence of the charge-transfer resistance (R_{CT}) on electrode potentials for the electro-oxidation of formic acid at the Au/FePt electrode by fitting the experimental data (Fig. 3) with the equivalent circuits in Fig. 5. Symbols are experimental data and the line is for eye-guiding only.

five. At even more positive potentials (-0.2 to $+0.1$ V), R_{CT} remains positive and exhibits only a slow decrease with electrode potential. However, at $+0.3$ V $\leq E \leq +0.5$ V, R_{CT} becomes negative and decreases drastically with increasing electrode potential. This can be ascribed to the inductive behavior arising from the electro-oxidation of surface adsorbed CO species, as speculated above (Fig. 3 and 4). Further increase of the electrode potential to $+0.6$ V leads to the recovery of positive R_{CT}, which shows a weak dependence on electrode potential ($+0.6$ V $\leq E \leq +0.9$ V).

Conclusion

In this paper, the electro-oxidation of formic acid at FePt alloy nanoparticle surfaces was studied by electrochemical voltammetry and impedance spectroscopy. The Au electrode modified with FePt alloy nanoparticles after UVO treatment was successfully used as an electrocatalyst for the oxidation of formic acid in an acid electrolyte. The FePt nanoparticle-functionalized electrode exhibited comparable onset potential for formic acid oxidation. Thus, FePt nanoparticles will be an excellent electrocatalytic candidate in fuel cell applications. Voltammetric and EIS studies showed that the formic acid oxidation was affected by reaction intermediates adsorbed on the electrode surface. In this study, EIS was used in the investigation of the reaction kinetics and mechanism of electro-oxidation of formic acid. The variation of the reaction mechanism in different potential regions was attributed to the formation of different intermediates on the electrode surface. With the increase of electrode potential, it was observed that the kinetic behavior evolved from resistive to pseudo-inductive and then to inductive characteristics. At low potentials, formic acid dissociated spontaneously to produce the CO intermediate, which adsorbed readily onto the electrode surface. At more positive electrode potentials, chemisorbed hydroxyl was formed, which enhanced the oxidative removal of the adsorbed CO intermediate. These results will be of fundamental

importance in understanding the electrochemical mechanism for liquid organic fuel oxidation at different electrode potentials, and hence enhanced performance of fuel cell catalysts.

References

1 C. Lamy, A. Lima, V. LeRhun, F. Delime, C. Coutanceau and J. M. Leger, *J. Power Sources*, 2002, **105**, 283–296.
2 J. Willsau and J. Heitbaum, *Electrochim. Acta*, 1986, **31**, 943–948.
3 X. Wang, J. M. Hu and I. M. Hsing, *J. Electroanal. Chem.*, 2004, **562**, 73–80.
4 Y. W. Rhee, S. Y. Ha and R. I. Masel, *J. Power Sources*, 2003, **117**, 35–38.
5 R. Parsons and T. Vandernoot, *J. Electroanal. Chem.*, 1988, **257**, 9–45.
6 G. Q. Lu, A. Crown and A. Wieckowski, *J. Phys. Chem. B*, 1999, **103**, 9700–9711.
7 M. C. Zhao, C. Rice, R. I. Masel, P. Waszczuk and A. Wieckowski, *J. Electrochem. Soc.*, 2004, **151**, A131–A136.
8 V. M. Jovanovic, D. Tripkovic, A. Tripkovic, A. Kowal and J. Stoch, *Electrochem. Commun.*, 2005, **7**, 1039–1044.
9 H. Okamoto, W. Kon and Y. Mukouyama, *J. Phys. Chem. B*, 2004, **108**, 4432–4438.
10 J. D. Lovic, A. V. Tripkovic, S. L. J. Gojkovic, K. D. Popovic, D. V. Tripkovic, P. Olszewski and A. Kowal, *J. Electroanal. Chem.*, 2005, **581**, 294–302.
11 M. Gholamian and A. Q. Contractor, *J. Electroanal. Chem.*, 1990, **289**, 69–83.
12 T. Iwasita, X. H. Xia, E. Herrero and H. D. Liess, *Langmuir*, 1996, **12**, 4260–4265.
13 J. Jiang and A. Kucernak, *J. Electroanal. Chem.*, 2002, **520**, 64–70.
14 A. Capon and R. Parsons, *J. Electroanal. Chem. Interfacial Electrochem.*, 1973, **44**, 1.
15 S. Wasmus, D. A. Tryk and W. Vielstich, *J. Electroanal. Chem.*, 1994, **377**, 205–214.
16 A. Capon and R. Parsons, *J. Electroanal. Chem. Interfacial Electrochem.*, 1973, **44**, 239.
17 T. Frelink, W. Visscher and J. A. R. vanVeen, *Langmuir*, 1996, **12**, 3702–3708.
18 W. F. Lin, M. S. Zei, M. Eiswirth, G. Ertl, T. Iwasita and W. Vielstich, *J. Phys. Chem. B*, 1999, **103**, 6968–6977.
19 T. Iwasita, H. Hoster, A. John-Anacker, W. F. Lin and W. Vielstich, *Langmuir*, 2000, **16**, 522–529.
20 H. S. Wang, C. Wingender, H. Baltruschat, M. Lopez and M. T. Reetz, *J. Electroanal. Chem.*, 2001, **509**, 163–169.
21 K. W. Park, J. H. Choi, B. K. Kwon, S. A. Lee, Y. E. Sung, H. Y. Ha, S. A. Hong, H. Kim and A. Wieckowski, *J. Phys. Chem. B*, 2002, **106**, 1869–1877.
22 J. F. Drillet, A. Ee, J. Friedemann, R. Kotz, B. Schnyder and V. M. Schmidt, *Electrochim. Acta*, 2002, **47**, 1983–1988.
23 Y. Morimoto and E. B. Yeager, *J. Electroanal. Chem.*, 1998, **444**, 95–100.
24 F. Colmati, E. Antolini and E. R. Gonzalez, *Electrochim. Acta*, 2005, **50**, 5496–5503.
25 T. Page, R. Johnson, J. Hormes, S. Noding and B. Rambabu, *J. Electroanal. Chem.*, 2000, **485**, 34–41.
26 E. Antolini, J. R. C. Salgado and E. R. Gonzalez, *J. Electroanal. Chem.*, 2005, **580**, 145–154.
27 S. Motoo and M. Watanabe, *J. Electroanal. Chem.*, 1976, **69**, 429–431.

This journal is © the Owner Societies 2006

Phys. Chem. Chem. Phys., 2006, **8**, 2779–2786 | 2785

28 C. Roychowdhury, F. Matsumoto, P. F. Mutolo, H. D. Abruña and F. J. DiSalvo, *Chem. Mater.*, 2005, **17**, 5871–5876.

29 J. Y. Lee, P. Strasser, M. Eiswirth and G. Ertl, *Electrochim. Acta*, 2001, **47**, 501–508.

30 M. Baldauf and D. M. Kolb, *J. Phys. Chem.*, 1996, **100**, 11375–11381.

31 R. S. Jayashree, J. S. Spendelow, J. Yeom, C. Rastogi, M. A. Shannon and P. J. A. Kenis, *Electrochim. Acta*, 2005, **50**, 4674–4682.

32 L. B. Lai, D. H. Chen and T. C. Huang, *J. Mater. Chem.*, 2001, **11**, 1491–1494.

33 H. Yang, N. Alonso-Vante, J. M. Leger and C. Lamy, *J. Phys. Chem. B*, 2004, **108**, 1938–1947.

34 Y. X. Chen, A. Miki, S. Ye, H. Sakai and M. Osawa, *J. Am. Chem. Soc.*, 2003, **125**, 3680–3681.

35 S. Park, Y. Xie and M. J. Weaver, *Langmuir*, 2002, **18**, 5792–5798.

36 S. C. Chang, L. W. H. Leung and M. J. Weaver, *J. Phys. Chem.*, 1990, **94**, 6013–6021.

37 T. Yajima, H. Uchida and M. Watanabe, *J. Phys. Chem. B*, 2004, **108**, 2654–2659.

38 H. Shiroishi, Y. Ayato, K. Kunimatsu and T. Okada, *J. Electroanal. Chem.*, 2005, **581**, 132–138.

39 H. A. Gasteiger, N. Markovic, P. N. Ross and E. J. Cairns, *J. Electrochem. Soc.*, 1994, **141**, 1795–1803.

40 H. N. Dinh, X. M. Ren, F. H. Garzon, P. Zelenay and S. Gottesfeld, *J. Electroanal. Chem.*, 2000, **491**, 222–233.

41 H. F. Oetjen, V. M. Schmidt, U. Stimming and F. Trila, *J. Electrochem. Soc.*, 1996, **143**, 3838–3842.

42 J. B. Goodenough, A. Hamnett, B. J. Kennedy, R. Manoharan and S. A. Weeks, *J. Electroanal. Chem.*, 1988, **240**, 133–145.

43 M. Watanabe, Y. M. Zhu and H. Uchida, *J. Phys. Chem. B*, 2000, **104**, 1762–1768.

44 H. Igarashi, T. Fujino, Y. M. Zhu, H. Uchida and M. Watanabe, *Phys. Chem. Chem. Phys.*, 2001, **3**, 306–314.

45 T. Toda, H. Igarashi, H. Uchida and M. Watanabe, *J. Electrochem. Soc.*, 1999, **146**, 3750–3756.

46 S. H. Sun, C. B. Murray, D. Weller, L. Folks and A. Moser, *Science*, 2000, **287**, 1989–1992.

47 R. Woods, in *Electroanalytical Chemistry*, ed. A. J. Bard, Marcel Dekker, Inc., New York, Vol. 9, 1976.

48 H. A. Gasteiger, N. Markovic, P. N. Ross and E. J. Cairns, *J. Phys. Chem.*, 1993, **97**, 12020–12029.

49 M. T. M. Koper, J. J. Lukkien, A. P. J. Jansen and R. A. van Santen, *J. Phys. Chem. B*, 1999, **103**, 5522–5529.

50 T. Iwasita, *Electrochim. Acta*, 2002, **47**, 3663–3674.

51 P. Waszczuk, T. M. Barnard, C. Rice, R. I. Masel and A. Wieckowski, *Electrochem. Commun.*, 2002, **4**, 599–603.

52 N. H. Li, S. G. Sun and S. P. Chen, *J. Electroanal. Chem.*, 1997, **430**, 57–67.

53 N. H. Li and S. G. Sun, *J. Electroanal. Chem.*, 1997, **436**, 65–72.

54 N. H. Li and S. G. Sun, *J. Electroanal. Chem.*, 1998, **448**, 5–15.

55 I. M. Hsing, X. Wang and Y. J. Leng, *J. Electrochem. Soc.*, 2002, **149**, A615–A621.

56 A. C. Chen, D. J. La Russa and B. Miller, *Langmuir*, 2004, **20**, 9695–9702.

57 Y. C. Liu, X. P. Qiu, W. T. Zhu and G. S. Wu, *J. Power Sources*, 2003, **114**, 10–14.

58 W. Sugimoto, K. Aoyama, T. Kawaguchi, Y. Murakami and Y. Takasu, *J. Electroanal. Chem.*, 2005, **576**, 215–221.

59 G. Markovich, C. P. Collier and J. R. Heath, *Phys. Rev. Lett.*, 1998, **80**, 3807–3810.

60 D. D. Macdonald, *Electrochim. Acta*, 1990, **35**, 1509–1525.

61 J. T. Muller, P. M. Urban and W. F. Holderich, *J. Power Sources*, 1999, **84**, 157–160.

62 A. Maritan and F. Toigo, *Electrochim. Acta*, 1990, **35**, 141–145.

63 R. E. Melnick and G. T. R. Palmore, *J. Phys. Chem. B*, 2001, **105**, 1012–1025.

2786 | *Phys. Chem. Chem. Phys.*, 2006, **8**, 2779–2786

This journal is © the Owner Societies 2006